II International Conference on Particle-based Methods – Fundamentals and Applications
PARTICLES 2011
E. Oñate and D.R.J. Owen (Eds)

ELEMENT TEST EXPERIMENTS AND SIMULATIONS: FROM DRY TOWARDS COHESIVE POWDERS

O. I. IMOLE, N. KUMAR AND S. LUDING

Multi-Scale Mechanics, TS, CTW
University of Twente
P.O. Box 217, 7500 AE Enschede, The Netherlands
e-mail: o.i.imole@ctw.utwente.nl, s.luding @utwente.nl, www.utwente.nl/ctw/msm

Key words: DEM, Element tests, Contact Models, Cohesive Powders, Uniaxial Compression, deviatoric stress.

Abstract. Findings from experiments and particle simulations for dry and cohesive granular materials are presented with the goal to reach quantitative agreement between simulations and experiments. Results for the compressibility, tested with the FT4 Powder Rheometer are presented. The first simulation results involve the strain controlled uniaxial compression of frictionless polydisperse spheres in a biaxial box using a linear visco-elastic contact model.

As main result, the evolution of pressure as a function of volume fraction is reported. Our anisotropic, uniaxial findings compare astonishingly well with results for purely isotropic compression. Concerning the second stress response, namely anisotropy, we present the evolution of the deviatoric stress as a function of the volume fraction, which cannot be measured with the FT4 experiment, but requires a bi-axial experiment.

1 INTRODUCTION

Cohesive powders pose a lot of challenge in various industrial applications for storage, transport and bulk handling. A full understanding of their flow behaviour still remains a challenging problem. It is also known that the bulk behaviour of cohesive powders depend on the contact properties of their constituents. In order to obtain information about the material behaviour, laboratory element test are performed with a control of the stress orstrain path. Alternatively, the Discrete Element Method (DEM) also provides information on the local micro-structure of powder systems.

It has been shown in Ref. [2] that isotropic and deviatoric deformation modes are pure modes while the uniaxial deformation test derives from the superposition of an isotropic and a deviatoric test. On the other hand, the biaxial tests involve mixed stress- and strain-control instead of completely prescribed strains.

The first section describes the experimental procedure and results from compressibility tests to obtain the pressure-density relation. Next, we describe the simulation procedure and show the evolution of pressure under isotropic deformation.

2 EXPERIMENTAL SET-UP AND METHODOLOGY

The experimental equipment used in this work is the FT4 powder Rheometer (Freeman technology Ltd. UK) which has been described in Ref. [3]. The FT4 Rheometer measures flowability and processability aspects of powders. Standard accessories for the compressibility test include the 50mm diameter blade, the vented piston and the 50mm bore by 50mm diameter borosilicate test vessel. One advantage of the FT4 Rheometer is the automated nature of the test procedure requiring minimal operator intervention apart from during sample preparation. A pre-conditioning cycle using the test equipment's automatic 'conditioning' procedure precedes the actual compressibility test. The procedure involves the gentle movement of the conditioning blade into the test sample to gently disturb the powder bed for a user pre-defined number of cycles. This action creates a uniform, lightly packed test sample that can be readily reproduced [4]. In this study, we allow three pre-conditioning cycles before the compressibility tests are carried out.

The compressibility tests are performed on two different food powder samples, which for the sake of brevity are not analyzed beyond the few specifications given in Table 1, but are just referred to as samples I and II. Size distribution is obtained by the 'dry dispersion module' of the Malvern Mastersizer 2000 (Malvern Instruments Ltd., UK) while the particle density is obtained by helium pycnometry. The specific surface area is also deduced from the Malvern PSD report. The distinguishing feature of these two samples is the percentage fat content with sample II being the powder with the lower fat content, and thus weaker expected cohesion. Obviously, the fat content influences the cohesivity of the powders with samples with higher fat showing more cohesion. As stated earlier, the samples are allowed to undergo three conditioning cycles after which the samples undergo a uniaxial compression from near 0 kPa to a maximum pressure of 20 kPa. For each test, the piston penetration depth, the normal stress, bulk density and compressibility (according to the Carr Index) are automatically recorded by the test program. A more detailed description of the test procedure is reported in [5].

Material property		**Unit**	**Sample I (strongly cohesive)**	**Sample II (moderately cohesive)**
Size distribution	(x_{10})	μm	12.783	3.119
	(x_{50})	μm	24.236	8.678
	(x_{90})	μm	47.579	22.540
Particle Density		kg/m³	1436	1509
Specific surface area		m²/g	0.284	1.414

Table 1. Material properties data for powder samples

The result from the compressibility test of samples I and II are shown in Fig 1, where pressure is plotted against bulk density (left) and against dimensionless volume fraction defines as ratio of granular volume to the total system volume (right). The more cohesive sample I behave differently from sample II with respect to both initial density and slope of the pressure-volume fraction curve of the sample. The sample with lower fat content has a smaller initial density at the commencement of the test and subsequently different bulk density values at the same pressure levels as the other sample. The effect of cohesion can also be seen from

the slope of the two plots, i.e., the sample with higher cohesion displays larger slope (resistance to uniaxial compression). It is not expected that the powder with higher fat content (most cohesive) powder is showing higher density. The fact is that the higher fat content has not only different contact properties, but also a different size distribution etc. So the material is different in (at least) two respects, and that might explain the unexpected density behavior. This behavior of cohesive powders will be studied in more detail in the future.

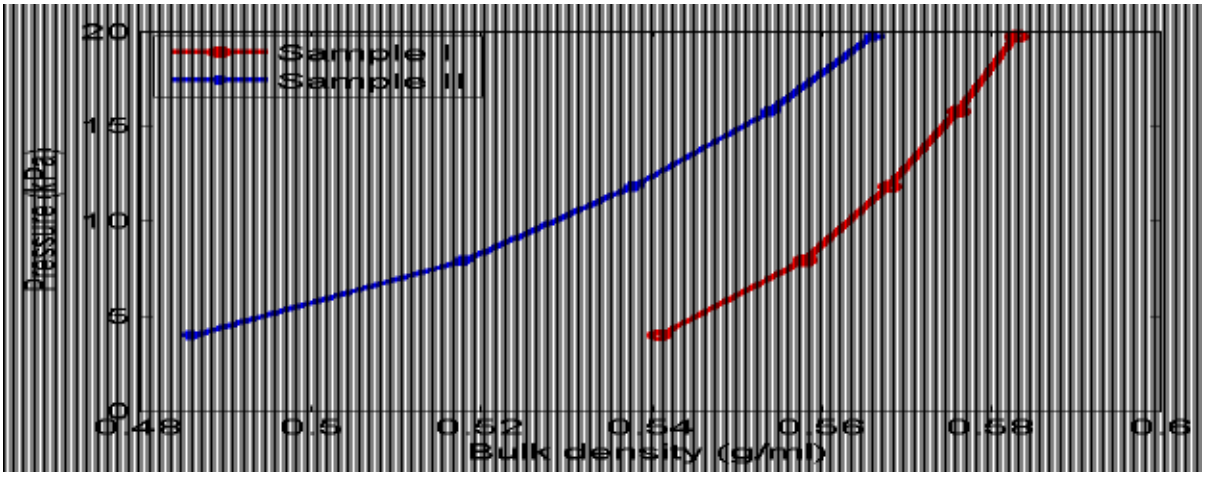

Fig. 1a: Plot of pressure as a function of the bulk density for the experimental samples. Fig. 1b. Plot of pressure as a function of the dimensionless volume fraction (bulk density scaled with the particle density) for the experimental samples.

Detailed study of various material parameters, including friction, rolling resistance and contact-adhesion in Refs. [7,14,15,16], where volume fractions slightly larger than 0.4 were reported, indicate that the range of experimentally observed volume fractions is quite challenging to achieve with DEM simulations and requires future work.

3 SIMULATION PROCEDURE

The Discrete Element Method (DEM) [6] was used to perform simulations in a bi-axial box. One advantage of the bi-axial box is the possibility of realizing different deformation modes with a single test experiment with a direct control of stress and strain [2,9]. In addition, laboratory experiments with the biaxial box are also feasible [8,9].

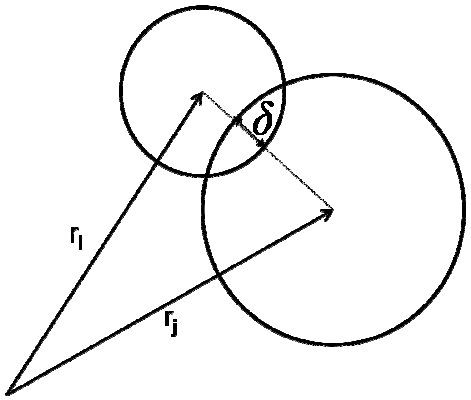

Fig. 2. Two particle contact with overlap δ

As a start-up and for initial simplicity, a linear visco-elastic contact model shown in equation (1) below determines the particle contact forces in the normal direction. In order to reduce dynamical effects and shorten relaxation times, an artificial viscous background dissipation γ_b proportional to the particle velocity is added, resembling the damping due to a background medium.

$$f^n = k\delta + \gamma\dot{\delta} \quad (1)$$

where k is the spring stiffness, δ as the overlap between particle contacts (as shown in Fig.2) and $\dot{\delta}$ is the relative velocity in the normal direction.

3.1 Simulation parameters

Simulation parameters are, system size $N = 4913$ particles, density ρ = 2000 [kg/m^3], elastic stiffness k_n = 10^5 [kg/s^2], particle damping coefficient γ = 1 [kg/s], background dissipation γ_b = 0.1 [kg/s]. The work of [7] provides a description of these artificial units and how they can be rescaled to fit values obtained from experiments due to the simplicity of the contact model used. It should also be noted that system has average particles radius <r> = 1 [mm], with polydispersity quantified by the width $w = r_{max}/r_{min} = 3$ of a uniform distribution defined in [1] where r_{max} and r_{min} are the radius of the biggest and smallest particles respectively.

3.2 Initial configuration

The initial configuration is such that particles were randomly generated in a 3D box and isotropically compressed to a volume above the jamming volume fraction v_0= 0.67. The isotropic compression stage is taken as the conditioning or preparation stage before the initiation of the test. Uniaxial compression is subsequently initiated at this point after allowing sufficient relaxation of the isotropic system. The volume fraction increases with time during compression to a maximum of v_{max} =0.82 and back to the original v_0 (Fig. 3a).

In theory, jamming occurs at the isostatic point [1,10,11,12]. The definition of an isostatic packing excludes all particles that do not belong to the force network, i.e. particles with exactly zero contacts are excluded. Nevertheless, in addition to the particles with zero contacts, there may be particles having some finite number of contacts for some short time, which do not contribute to the mechanical stability of the packing. These particles (and those

with zero contacts) are called *rattlers*. The contacts of these rattlers are transient because the repulsive contact forces push them away from the mechanically stable backbone [1]. While it is possible to check numerically the contribution of every particle to the force network [13], a less rigorous way to identify rattlers is to just count their contacts. Since frictionless particles with less than four contacts are not mechanically stable in 3 dimensional systems, they are defined as rattlers. To exclude rattlers from the system, the definition of the classical coordination number i.e. average number of contacts per particle is modified to become

$$C := C^m = \frac{M_4}{N} \tag{2}$$

where M_4 is the number of contacts of particles with at least four contacts and N is the total number of particles. The corrected coordination number, defined as $C^* := \frac{M_4}{N_4}$ where N_4 is the number of particles with at least four contacts has value equal to 6 at the isostatic point in 3 dimensions. We do not suggest that this definition of coordination number is valid for all real powders - only a starting point for frictionless materials. We use these definitions of coordination numbers to find the pressure-volume fraction relation that is discussed in next section.

Above the jamming volume fraction, contacts between the particles are deformed more and more with increasing confining pressure. The potential energy is an indicator of the overlap between particles hence its values are considerably larger than the kinetic energy above jamming (Fig. 3(b)). Relatively lower potential energy values below the jammed state (fluid state) have been reported in [1]. Hence, the ratio of the potential energy values to the kinetic energy values gives a rough indication that the system is above the jamming regime in the quasi-static state. Lower energy ratios can be obtained by performing slower rate simulations as seen in Fig. 3(b).

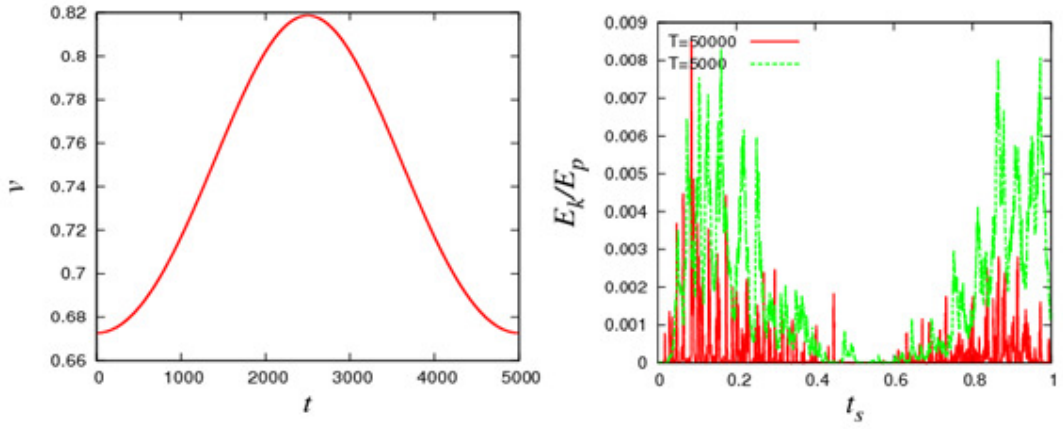

Fig. 3a: Evolution of volume fraction as a function of time (t) for isotropic compression. Fig. 3b. Comparison of ratio of kinetic energy to the potential energy in scaled time (t_s=t/T) for two uniaxial compression simulations where T is the period of one compression-decompression cycle ($E_k/E_p < 0.1$ percent). The simulation represented by the red curve is 10 times slower than the green.

3.3 Evolution of pressure under isotropic deformation

In this section, the relation between pressure and volume fraction is studied. The non-dimensional pressure [1] is defined as:

$$p = \frac{2\langle r \rangle}{3k_n} tr(\sigma) \tag{3}$$

where $tr(\sigma)$ is the trace of the averaged stress tensor. The normalized average overlap, $\langle \Delta \rangle_c = \delta_c / \langle r \rangle$ is related to the volumetric strain under the simplifying assumption of uniform deformation in the packing as:

$$d\langle \Delta \rangle_c = D\epsilon_v \tag{4}$$

where $\epsilon_v = \epsilon_{ii}$ is the trace of the infinitesimal strain tensor and D is a proportionality constant that depends on the size distribution. The integral of ϵ_v, denoted by ε_v is the true logarithmic volume change of the system relative to the reference volume V_0, with corresponding reference volume fraction, v_0 which is chosen without loss of generality to be equal to the critical, jamming volume fraction $v_0 = v_c$, so that the average normalized overlap:

$$\langle \Delta \rangle_c = D \int_{V_0}^{V} \epsilon_v = D\varepsilon_v = Dln\frac{v_c}{v} \tag{5}$$

The non-dimensional pressure equation becomes:

$$p = p_0 \frac{vC}{v_c}(-\varepsilon_v)\left[1 - \gamma_p(-\varepsilon_v)\right] \tag{6}$$

and the scaled pressure is given as:

$$p^* = \frac{pv_c}{vC} = p_0(-\varepsilon_v)\left[1 - \gamma_p(-\varepsilon_v)\right] \tag{7}$$

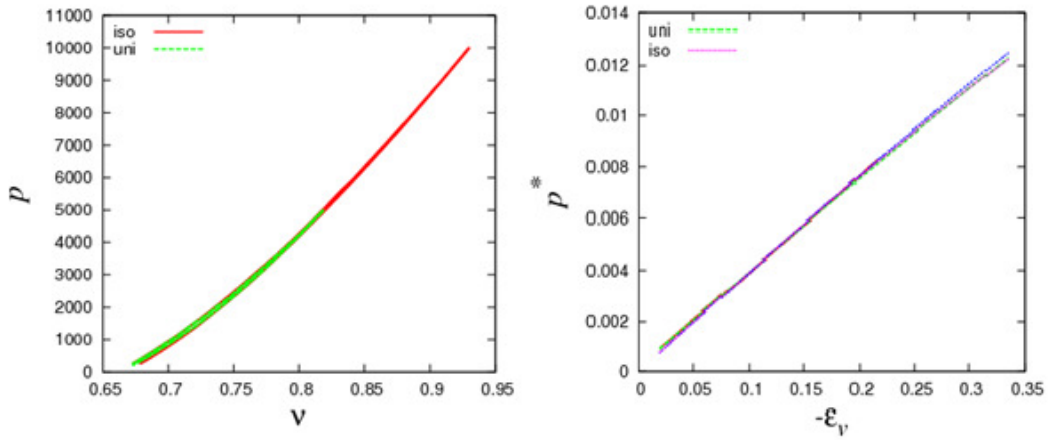

Fig. 4(a). Total pressure (dimension $\mathrm{Kg/mm.s^2}$) as a function of the volume fraction for the loading and unloading cycle Fig. 4(b). The scaled pressure as a function of the (negative) volumetric strain for the unloading cycle for an isotropic [1] and our uniaxial dataset (right).

Fig. 4(a) shows the total pressure (dimensional) as a function of the volume fraction during the loading and unloading cycles for a purely isotropic data set and our uniaxial simulation. As seen, the pressure curve during the unloading cycle shifts to the right due to hysteretic effects. Fig 4(b) shows the scaled pressure as a function of the (negative) volumetric strain with v_c=0.665 for a comparable isotropic compression data set and the uniaxial compression set being studied. Astonishingly, analytical prediction of the scaled pressure as a function of volumetric strain for an isotropic system compares well with our uniaxial simulation where the particles are frictionless.

Other deformation rates studied collapse with the same curve for small deformations. The scaled pressure is also well represented by the linear relation $\mathrm{p}^* \approx -\mathrm{p}_0\varepsilon_\mathrm{v}$ in Eq. (6) for small deformations. The best fit quality for pressure-strain curve for the unloading cycle is obtained when Eq. (7) is used to fit the pressure disregarding the data close to jamming since those are not reliable due to dynamic effects.

For both cases (isotropic and uniaxial), the coefficients $\mathrm{p}_0 \approx 0.039$, $\gamma_\mathrm{p} \approx 0.011$ and $\mathrm{v_c} \approx 0.665$ fit our data well with errors less than one percent for all densities.

3.4 Deviatoric stress

The average isotropic stress (pressure) is defined as:

$$p = \frac{\sigma_{xx} + \sigma_{yy} + \sigma_{zz}}{3}. \tag{8}$$

The deviatoric stress between the moving boundary (wall with normal in z-direction) and the fixed periodic boundary walls is defined by:

$$\sigma_{DEV1} = \sigma_{zz} - \frac{\sigma_{xx} + \sigma_{yy}}{2} \tag{9}$$

Also, we define the second deviatoric stress, σ_{DEV2} between the fixed periodic boundary directions in the system as:

$$\sigma_{DEV2} = \frac{\sigma_{xx} - \sigma_{yy}}{2}. \tag{10}$$

The first deviatoric stress (σ_{DEV1}) quantifies the (stress) anisotropy between the compression/de-compression direction and the non-deformed direction, while the second deviatoric stress (σ_{DEV2}) quantifies the anisotropy between the two equivalent non-deformed directions-which should be small for symmetry reasons. Fig. 5 shows the evolution of the deviatoric stress during loading and unloading. In order to compare the magnitude of $\sigma_{DEV1}$and σ_{DEV2} we normalize them with the isotropic pressure p and plot this as a function of the volume fraction.

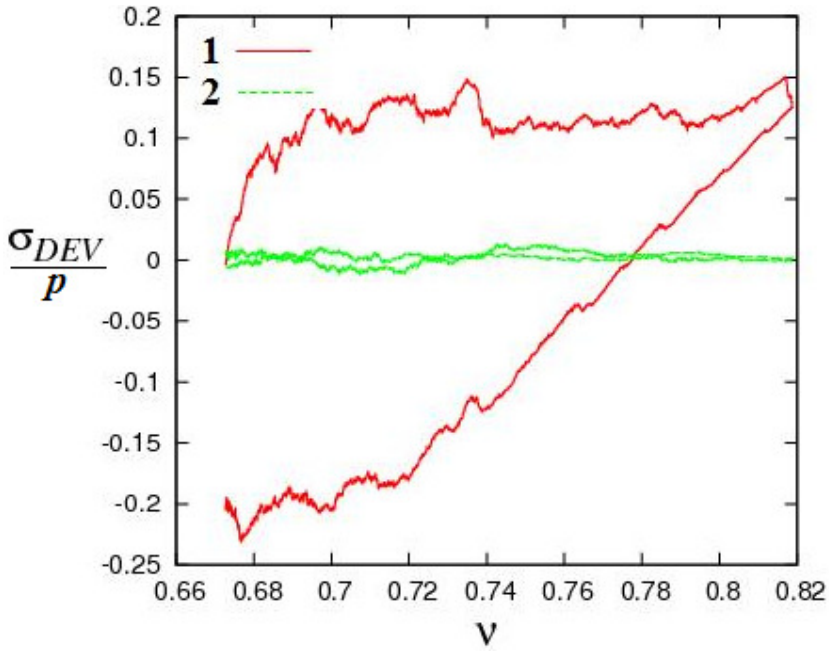

Fig. 5: Evolution of the deviatoric stress as a function of volume fraction.

The second deviatoric stress variation between the fixed periodic walls in the *x* and *y* plane lies close to zero during the loading and unloading cycles reflecting the symmetry in *x*-*y*-directions. In contrast, σ_{DEV1} shows some interesting profile. The stress increases up to ≈ 0.12 (12 ± 2 percent) from the commencement of the loading cycle and thereafter remains fairly constant till the end of the loading cycle. During unloading, it decreases almost linearly until it gets to the isotropic state ($\frac{\sigma_{DEV}}{p} = 0$) and goes down further to ≈ -0.2 (-20 ± 2 percent) relative to the start-up point. Interestingly, the isotropic-stress is not recovered when the initial value of valume fraction is reached. That is the system stays anisotropic after the complete cyclic path.

4 CONCLUSION

We have presented results from a compressibility test on two cohesive powder samples. Our experiments show effects of the fat content (cohesivity) on the pressure-density curve. Simulation results from the strain controlled uniaxial compression of frictionless polydisperse spheres have also been presented. An important result in this study is the agreement obtained for the analytical prediction of the scaled pressure as a function of volumetric strain for a purely isotropic system and our uniaxial simulation. For our system, this suggests an advantage of the 'cheaper' uniaxial compression over isotropic deformation. Compression is done in one direction in the former while the three walls have to be moved simultaneously in the latter. The second observation is the confirmation of symmetry in the two non-mobile directions, and the observation of particular stress anisotropy between the moving and non-moving direction.

The overall goal of this research is towards cohesive powder modelling with the discrete element method. Therefore the work presented here is the 'start-point' to achieve agreement between experiments and simulation. Parameter studies with isotropic test configuration [7,14,15,16] have been performed already and have to be complemented by similar studies with uniaxial configuration – first to parallel the experiments, and second to activate anisotropy. More realistic contact models to incorporate friction and cohesion need to be implemented and physical experiments on cohesive powders with the bi-axial box needs to be performed. Agreement obtained for the analytical prediction of the scaled pressure as a function of the volume fraction will be investigated for more realistic contact models. In addition, the use of simulation parameters obtained from physical experiments will be examined. Simulations and theory on different deformation modes [2] also need to be fine-tuned, other loading paths that can be realised in the bi-axial box are currently being studied.

ACKNOWLEDGEMENT

Helpful discussions with V. Magnanimo, M. Ramaioli (Nestle Research Centre, Lausanne) and E. Chavez (Nestle PTC, Orbe) are gratefully acknowledged. This work is financially supported by the research programme of "PARDEM", under the Marie Curie ITN, European Union.

REFERENCES

[1] Göncü, F., O. Duran, and S. Luding, Constitutive relations for the isotropic deformation of frictionless packings of polydisperse spheres, C. R. Mecanique 338, 570-586, 2010.
[2] Luding, S., and S. Perdahcioglu, A local constitutive model with anisotropy for various homogeneous 2D Biaxial deformation modes, CIT 83(5), 672-688, 2011.
[3] Freeman R., The Importance of Air content on the Rheology of Powders – An Empirical Study Using the FT4 Powder Rheometer, 2003.
[4] Freeman R., Measuring the flow properties of consolidated, conditioned and aerated powders – a comparative study using a powder Rheometer and a rotational shear cell.

Powder Technology 174 25 – 33 (2007).
[5] Freeman, R, (2003), The importance of air content on the rheology of powders – an empirical study using the FT4 Powder Rheometer. American Laboratory News - November 2004.
[6] Cundall P.A., Strack, O.D.L., A discrete numerical model for granular assemblies. In Geotechnique, vol. 29, pp. 47-65, 1979.
[7] Luding, S., "Cohesive, frictional powders: contact models for tension," Granular matter, vol. 10, no. 4, 2008.
[8] Roeck M.; Morgeneyer M., Schwedes J., Brendel L., Wolf D. E., Kadau D.: Visualization of Shear Motions of Cohesive Powders in the True Biaxial Shear Tester. Volume 26, Issue 1, Pages 43 – 54, 2008.
[9] Tykhoniuk R., Tomas J., Luding S., Kappl M., Heim L., Hans-Jürgen Butt. Chem. Eng. Sci. Volume 62, Issue 11, Pages 2843-2864, June 2007.
[10] O'Hern, C. S., Silbert L. E., Liu A. J., and Nagel S. R., "Jamming at zero temperature and zero applied stress: The epitome of disorder," Phys. Rev. E, vol. 68, no. 1, Part 1, 2003.
[11] Silbert, L. E., Ertas D., Grest G. S., Halsey T. C., and Levine D., "Geometry of frictionless and frictional sphere packings," Phys. Rev. E, vol. 65, p. 051302, Mar. 2002.
[12] O'Hern, C. S., Langer S. A., Liu A. J., and Nagel S. R., "Random packings of frictionless particles," Phys. Rev. Lett., vol. 88, no. 7, 2002.
[13] Kruyt, N. P., "Three-dimensional lattice-based dispersion relations for granular materials," in IUTAM-ISIMM Symposium on Mathematical Modeling and Physical Instances of Granular Flows (J. Goddard, P. Giovine, and J. T. Jenkins, eds.), (Reggio Calabria (Italy), 14.18 September 2009), pp. 405–415, AIP, 2010.
[14] Luding S., Bauer E., "Evolution of swelling pressure of cohesive-frictional, rough and elasto-plastic granulates," in Geomechanics and Geotechnics: From Micro to Macro, (IS-Shanghai Conference Proceedings, 10.-12. Oct. 2010).
[15] Gonzalez S., Thornton A. R., and Luding S., "An event driven algorithm for fractal cluster formation", in: CCP2010 Proceedings pp. 105-106. (Trondheim, Norway, June 23-26, 2010).
[16] Thornton C., "Numerical simulations of deviatoric shear deformation of granular media" in Geotechnique, 50(1):43–5, 2000.